Influence of Ice Particle Surface Roughening on the Global Cloud Radiative Effect

BINGQI YI,* PING YANG,* BRYAN A. BAUM,[+] TRISTAN L'ECUYER,[#] LAZAROS OREOPOULOS,[@]
ELI J. MLAWER,[&] ANDREW J. HEYMSFIELD,[**] KUO-NAN LIOU[++]

*Department of Atmospheric Sciences, Texas A&M University, College Station, Texas
[+]Space Science and Engineering Center, University of Wisconsin–Madison, Madison, Wisconsin
[#]Department of Atmospheric and Oceanic Sciences, University of Wisconsin–Madison, Madison, Wisconsin
[@]Climate and Radiation Laboratory, NASA Goddard Space Flight Center, Greenbelt, Maryland
[&]Atmospheric and Environmental Research, Lexington, Massachusetts
[**]National Center for Atmospheric Research, Boulder, Colorado
[++]Joint Institute for Earth System Science and Engineering, and Department of Atmospheric and Oceanic Sciences,
University of California, Los Angeles, Los Angeles, California

ABSTRACT

Ice clouds influence the climate system by changing the radiation budget and large-scale circulation. Therefore, climate models need to have an accurate representation of ice clouds and their radiative effects. In this paper, new broadband parameterizations for ice cloud bulk scattering properties are developed for severely roughened ice particles. The parameterizations are based on a general habit mixture that includes nine habits (droxtals, hollow/solid columns, plates, solid/hollow bullet rosettes, aggregate of solid columns, and small/large aggregates of plates). The scattering properties for these individual habits incorporate recent advances in light-scattering computations. The influence of ice particle surface roughness on the ice cloud radiative effect is determined through simulations with the Fu–Liou and the GCM version of the Rapid Radiative Transfer Model (RRTMG) codes and the National Center for Atmospheric Research Community Atmosphere Model (CAM, version 5.1). The differences in shortwave (SW) and longwave (LW) radiative effect at both the top of the atmosphere and the surface are determined for smooth and severely roughened ice particles. While the influence of particle roughening on the single-scattering properties is negligible in the LW, the results indicate that ice crystal roughness can change the SW forcing locally by more than $10\,\mathrm{W\,m^{-2}}$ over a range of effective diameters. The global-averaged SW cloud radiative effect due to ice particle surface roughness is estimated to be roughly 1–$2\,\mathrm{W\,m^{-2}}$. The CAM results indicate that ice particle roughening can result in a large regional SW radiative effect and a small but nonnegligible increase in the global LW cloud radiative effect.

1. Introduction

Ice clouds significantly influence the radiation budget of the climate system (Liou 1986; Lynch et al. 2002; Baran 2009; and references therein) and also influence the large-scale circulations in the atmosphere (Hartmann et al. 1992). The quantification of the radiative effects of ice clouds has been the objective of numerous studies from both satellite-/ground-based observations and numerical modeling (e.g., Platt et al. 1998; Comstock et al. 2002; Yang et al. 2007; Lee et al. 2009; Baran 2012; and

references therein). However, owing to various uncertainties, ice clouds still remain one of the least known components in the atmospheric system. The uncertainties are caused by many factors, from microphysical properties, such as the range of particle size distributions (PSD) with their associated crystal shapes (habits), to optical properties such as extinction coefficient, phase matrix, single-scattering albedo, and asymmetry factor. Modeling studies by Slingo and Slingo (1988, 1991) show significant sensitivity of climate models to the cloud radiative effect. Thus, it is imperative to accurately represent both ice cloud microphysical and optical properties in atmospheric numerical models.

Many ice cloud optical property parameterization schemes have been suggested for use in atmospheric models. Early schemes parameterized optical properties

Corresponding author address: Dr. Ping Yang, Department of Atmospheric Sciences, Texas A&M University, TAMU-3150, College Station, TX 77843.
E-mail: pyang@tamu.edu

as functions of temperature based only on limited observations (e.g., Platt and Harshvardhan 1988). By assuming ice particles to have spherical shape that is the same as liquid clouds (Slingo 1989), the optical properties of ice clouds were derived from the Lorenz–Mie theory. It soon became apparent that the Lorenz–Mie solution was inadequate for representing the scattering and absorbing properties of nonspherical ice particles because ice cloud particle shapes are complex. Takano and Liou (1989) used smooth-faceted hexagonal columns as the ice crystal model of choice and developed a parameterization scheme based on this habit. Ebert and Curry (1992) also employed the hexagonal column model and parameterized ice cloud optical properties as functions of ice water path and the effective particle radius. Fu and Liou (1993) developed a parameterization for use in their own radiative transfer code, which has subsequently been updated (Fu 1996; Fu et al. 1998). In the Community Earth System Model (CESM), which uses the general circulation model version of the radiation code in the Rapid Radiative Transfer Model (RRTM) (known as RRTMG), the ice cloud optical property parameterization (Mitchell et al. 1996, 2006) is based on a combination of the anomalous diffraction theory (ADT) approximation and a database by Yang et al. (2000). Hong et al. (2009) developed a new parameterization for ice cloud bulk optical properties as a function of effective particle size for use in climate models based on six ice habits and observed ice particle size distributions from several field campaigns, again assuming smooth particle surfaces. It is important to note that the evolution in parameterization scheme development has been toward the use of more ice particle habits and more realistic ice particle size distributions, but with limited consideration of surface roughness. One of the exceptions is Edwards et al. (2007), whose parameterization scheme using an ice aggregate model accounts for roughened surfaces and was implemented in the Third Hadley Centre Atmosphere Model (HadAM3) GCM.

A focus of recent research has been on uncertainty reduction in ice cloud properties as more field campaign data become available (Heymsfield et al. 2010, 2013) from both hemispheres. Additionally, theoretical advances help to simulate ice particle optical properties more accurately by including more sophisticated ice particle shapes and considering ice surface roughness (Yang et al. 2000, 2003; Zhang et al. 2004; Yang et al. 2008; Zhang et al. 2009). How the findings from these observational and theoretical advances influence ice cloud radiative effect is the focal point of this study, specifically the influence of ice particle surface roughness on radiative transfer and climate simulations.

Ice particles are most likely not pristine and may include air bubbles, internal fractures, and other inhomogeneities. In situ observations indicate that ice particles tend to have rough surfaces owing to the evaporation, sublimation, or riming processes (Cross 1969; Ono 1969; Davy and Branton 1970; Ulanowski et al. 2006, 2012). It is still unknown how ubiquitous the surface roughness feature is among ice cloud particles. Previous studies have shown the importance of ice particle surface roughness effects and the need for them to be accounted for in the computation of the ice cloud radiative effect (Macke 1993; Yang and Liou 1998). Fu (2007) considers the ice surface roughness effect on the asymmetry factor and treats it by neglecting the contribution from delta transmission, obtaining an approximate $20\,\mathrm{W\,m^{-2}}$ impact on the reflected solar flux. A recent study by Yang et al. (2012) shows 10–$15\,\mathrm{W\,m^{-2}}$ differences in upward and downward solar fluxes owing to an assumed reduction in the asymmetry factor induced by ice particle roughness. The primary shortcoming of the previous studies is an oversimplified representation of ice particle surface roughness. Another shortcoming is the application of single-column radiative transfer codes to a limited number of individual cases, thereby limiting the representativeness of the results. These earlier studies helped, however, establish the need to update the effects of ice crystal roughness on optical property parameterizations and to revisit the radiative forcing estimates. Both issues are pursued comprehensively in this paper. We describe the data and methodology used in this study in section 2. Section 3 shows the simulated ice roughness effects by single-column radiative transfer models (RTMs) and an AGCM. A summary and conclusions are given in section 4.

2. Data and methodology

a. Ice particle single-scattering-property database

In this study, the single-scattering properties for nine ice particle habits from the ultraviolet to the far IR are provided in a library recently developed by Yang et al. (2013). The library is developed using the most up-to-date ice refractive index values (Warren and Brandt 2008) currently available. The habits are those most often found in clouds and include droxtals, plates, solid and hollow columns, solid and hollow bullet rosettes, an aggregate of solid columns, and a small/large aggregate of plates. The calculations implement a new treatment of forward scattering (Bi et al. 2009) that considers the ray-spreading effect more accurately. With this new treatment, the delta-transmission term is no longer

necessary. What makes the library optimal for use here is the availability of three ice particle surface roughness conditions for each habit: completely smooth, moderately roughened, and severely roughened, following the approximate approach discussed in Yang et al. (2008). The method of particle surface roughness treatment can be found in the appendix. The severely roughened ice particles compare best with global Cloud-Aerosol Lidar with Orthogonal Polarization (CALIOP) backscattering data (Baum et al. 2011) and also with *Polarization and Anisotropy of Reflectances for Atmospheric Sciences Coupled with Observations from a Lidar* (*PARASOL*) data (C.-Labonnote et al. 2001; Cole et al. 2013). Our approach in this paper is to perform calculations for the completely smooth and the severely roughened cases (referred to as "CS case" and "SR case," respectively), and quantify resulting flux differences as the surface roughness effect.

b. Microphysical data and ice habit mixture

A total of 14 408 particle size distributions (PSDs) derived from 11 field campaigns carried out in different locations are used in this study. Heymsfield et al. (2013) describe the data in more detail. The microphysical data were reprocessed where necessary to mitigate the ice particle shattering effect on the PSDs. A general habit mixture scheme is adopted that uses all nine habits (Baum et al. 2011). The same ice habit mixture scheme is adopted in remote sensing studies of ice cloud using CALIOP (Baum et al. 2011) and *PARASOL* (Cole et al.

2013). These microphysical data are used for the calculation of the bulk scattering properties for the individual shortwave (SW) and longwave (LW) bands of the RTMs.

c. Calculation of the ice cloud bulk scattering properties

The method to calculate the ice cloud bulk scattering properties follows previous studies (Baum et al. 2005, 2011). The effective particle diameter (Foot 1988; Yang et al. 2000; Mitchell 2002) is defined as

$$
D_{\text{eff}} = \frac{3}{2} \frac{\sum\limits_{h=1}^{M} \left[\int_{D_{\min}}^{D_{\max}} V_h(D) f_h(D) n(D)\, dD \right]}{\sum\limits_{h=1}^{M} \left[\int_{D_{\min}}^{D_{\max}} A_h(D) f_h(D) n(D)\, dD \right]}, \quad (1)
$$

where D is particle maximum dimension, $D_{\min}$ and $D_{\max}$ are the minimum and maximum ice particle dimensions, V_h and A_h are the volume and area of an ice particle with habit h, M is the number of habits, f_h is the habit fraction of habit h that depends on the ice particle size, and n is the number distribution.

Band-averaged bulk optical properties of ice clouds are calculated by integration over both particle size and appropriate wavelength band limits. For this study, the mass extinction coefficient, the single-scattering albedo, and asymmetry factor over a band are provided by

$$
k_{\text{ext}} = \frac{\int_{\lambda_{\min}}^{\lambda_{\max}} \int_{D_{\min}}^{D_{\max}} \sum\limits_{h=1}^{M} [Q_{\text{ext},h}(D,\lambda) A_h(D) f_h(D)] S(\lambda) n(D)\, dD\, d\lambda}{\int_{\lambda_{\min}}^{\lambda_{\max}} \int_{D_{\min}}^{D_{\max}} \sum\limits_{h=1}^{M} [V_h(D) f_h(D)] S(\lambda) n(D)\, dD\, d\lambda}, \quad (2)
$$

$$
\overline{\sigma}_{\text{sca}} = \frac{\int_{\lambda_{\min}}^{\lambda_{\max}} \int_{D_{\min}}^{D_{\max}} \sum\limits_{h=1}^{M} [\sigma_{\text{sca},h}(D,\lambda) f_h(D)] S(\lambda) n(D)\, dD\, d\lambda}{\int_{\lambda_{\min}}^{\lambda_{\max}} \int_{D_{\min}}^{D_{\max}} \sum\limits_{h=1}^{M} [f_h(D)] S(\lambda) n(D)\, dD\, d\lambda}, \quad (3)
$$

$$
\overline{\sigma}_{\text{ext}} = \frac{\int_{\lambda_{\min}}^{\lambda_{\max}} \int_{D_{\min}}^{D_{\max}} \sum\limits_{h=1}^{M} [\sigma_{\text{ext},h}(D,\lambda) f_h(D)] S(\lambda) n(D)\, dD\, d\lambda}{\int_{\lambda_{\min}}^{\lambda_{\max}} \int_{D_{\min}}^{D_{\max}} \sum\limits_{h=1}^{M} [f_h(D)] S(\lambda) n(D)\, dD\, d\lambda}, \quad (4)
$$

$$
\overline{\omega}(\lambda) = \frac{\overline{\sigma}_{\text{sca}}(\lambda)}{\overline{\sigma}_{\text{ext}}(\lambda)}, \quad \text{and} \quad (5)
$$

TABLE 1. Spectral bands in the RRTMG and Fu–Liou RTMs.

RRTMG				Fu–Liou			
SW		LW		SW		LW	
Band	μm	Band	cm^{-1}	Band	μm	Band	cm^{-1}
16	3.08–3.85	1	10–350	1	0.2–0.7	1	0–280
17	2.5–3.08	2	350–500	2	0.7–1.3	2	280–400
18	2.15–2.5	3	500–630	3	1.3–1.9	3	400–540
19	1.94–2.15	4	630–700	4	1.9–2.5	4	540–670
20	1.63–1.94	5	700–820	5	2.5–3.5	5	670–800
21	1.3–1.63	6	820–980	6	3.5–4.0	6	800–980
22	1.24–1.3	7	980–1080			7	980–1100
23	0.78–1.24	8	1080–1180			8	1100–1250
24	0.63–0.78	9	1180–1390			9	1250–1400
25	0.44–0.63	10	1390–1480			10	1400–1700
26	0.34–0.44	11	1480–1800			11	1700–1900
27	0.26–0.34	12	1800–2080			12	1900–2200
28	0.2–0.26	13	2080–2250				
29	3.85–12.2	14	2250–2380				
		15	2380–2600				
		16	2600–3250				

$$g = \frac{\int_{\lambda_{\min}}^{\lambda_{\max}} \int_{D_{\min}}^{D_{\max}} \sum_{h=1}^{M} [g_h(D,\lambda)\sigma_{\mathrm{sca},h}(D,\lambda)f_h(D)]S(\lambda)n(D)\,dD\,d\lambda}{\int_{\lambda_{\min}}^{\lambda_{\max}} \int_{D_{\min}}^{D_{\max}} \sum_{h=1}^{M} [\sigma_{\mathrm{sca},h}(D,\lambda)f_h(D)]S(\lambda)n(D)\,dD\,d\lambda}, \tag{6}$$

where $\lambda_{\max}$ and $\lambda_{\min}$ are the upper and lower wavelength limits of a given SW/LW band, $\sigma_{\mathrm{sca},h}$ is the scattering cross section for habit h, $\sigma_{\mathrm{ext},h}$ is the extinction cross section for habit h, $Q_{\mathrm{ext},h}$ is the extinction efficiency, and $S(\lambda)$ is the solar spectrum (Chance and Kurucz 2010) for SW bands. For LW bands, the solar spectrum is replaced with the Planck function assuming a cloud temperature of 233 K. Note that these assumptions are adopted for practical reasons because the number of distinct in-atmosphere solar spectra and cloud temperatures is too large to consider all possible combinations. We find that the band-averaged optical properties are largely insensitive to these assumptions. Two cases of ice particle surface roughness (CS and SR) are considered separately. The influence of meteorological conditions (i.e., temperature and humidity) on ice particle surface roughness is not included in this study because the nature of these physical mechanisms is not sufficiently known.

d. The RTMs and AGCM

The bulk single-scattering properties are parameterized subsequently as functions of the effective particle diameter and implemented in the Fu–Liou and the RRTMG RTM codes and the Community Atmosphere Model (CAM5.1) AGCM. The Fu–Liou RTM has 6 solar bands and 12 IR bands; the RRTMG package (Iacono et al. 2008) has 14 solar bands and 16 IR bands. The spectral bands in the Fu–Liou and RRTMG RTMs are given in Table 1. Both use the correlated-k distribution method to treat absorption by atmospheric gases.

In the next section, results are presented for our new ice cloud models to demonstrate the flux differences caused solely by assumptions about particle roughness.

3. Results and discussions

a. Broadband RTM results

The differences in ice cloud optical properties between the CS and SR cases are shown in Fig. 1. The CS results show that the mass extinction coefficient decreases sharply with an increase in D_{eff} from 10 to 60 μm and remains under 0.05 m^2 g^{-1} for large ice particles. The various bands of both RTMs differ little with regard to the mass extinction coefficient of SR particles. As the central wavelength of the spectral band increases, the single-scattering albedo gradually decreases from 1 to smaller values, and thus becomes more sensitive to D_{eff}. The bands with shorter wavelengths have smaller asymmetry factors compared with those with longer wavelengths. Not surprisingly, there exist minimal differences
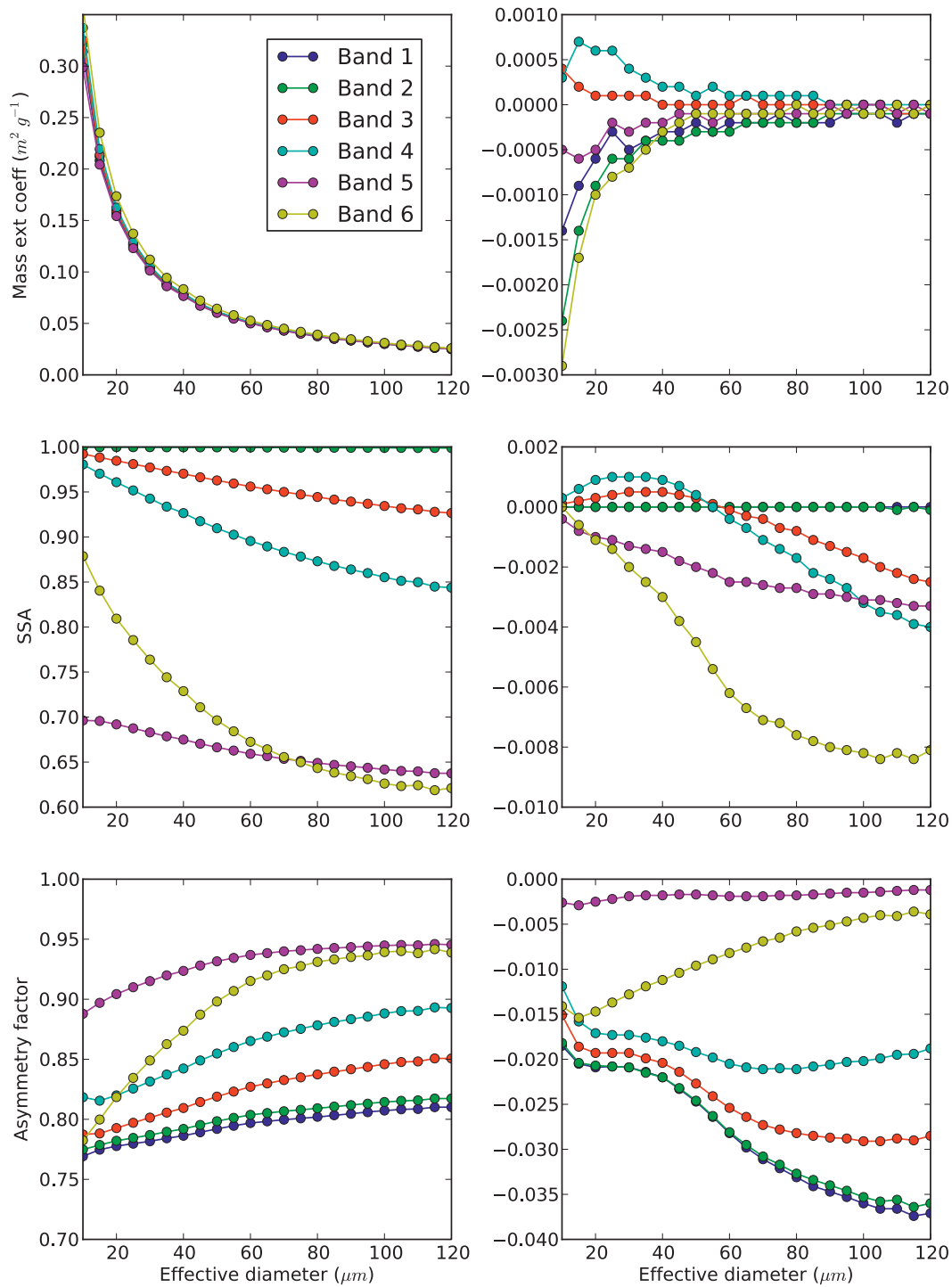
FIG. 1. (top) Mass extinction coefficient, (middle) single-scattering albedo, and (bottom) asymmetry factor as a function of effective diameter for (left) the Fu–Liou model solar bands for severely roughened ice particles. (right) Corresponding differences between the severely roughened and the smooth ice models. The six bands shown correspond to the Fu–Liou RTM SW bands in Table 1.
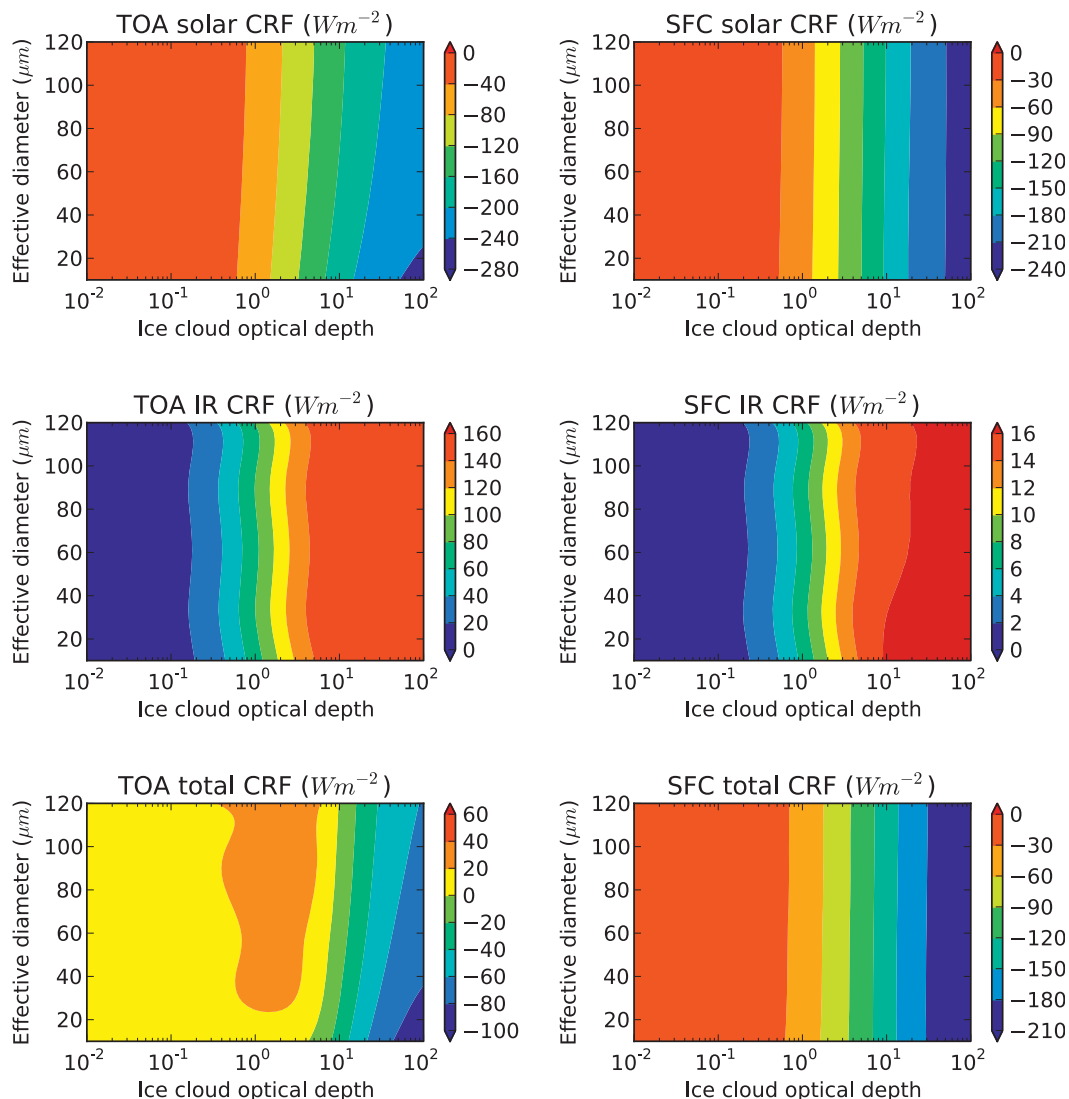
FIG. 2. (top) SW, (middle) LW, and (bottom) total cloud radiative forcing (CRF) at solar zenith angle (SZA) = 60° as a function of effective diameter and cloud optical thickness as simulated by the Fu–Liou RTM for SR ice particles at (left) the TOA and (right) the SFC.

between the SR and CS values for the mass extinction coefficient and the single-scattering albedo, while the asymmetry factor shows a much larger effect from roughening. Moreover, the SR ice particles have consistently lower asymmetry factors than the CS particles for the same D_{eff}. The differences between the SR and the CS cases generally increase with D_{eff} with the exception of bands 5 and 6. Compared with the near-IR bands, the shorter wavelength bands (bands 1–4) show much larger differences in asymmetry factor between the SR and CS cases. This is consistent with previous studies showing that the effect of ice particle surface roughness is mostly realized as a reduction in the asymmetry factor; that is, the CS particles scatter more

in the forward direction than the SR particles. For the mass extinction coefficient, bands 2 and 6 exhibit the largest SR–CS difference when D_{eff} is small. Band 6 also exhibits the largest SR–CS difference in the single-scattering albedo when D_{eff} is large.

A test case is designed to illustrate the sensitivity of cloud radiative effect to ice particle surface roughness in the two RTMs using a common standard midlatitude summer atmospheric profile for clear- and cloudy-sky simulations. The cloud radiative effect (CRE) is defined as the difference in the net (SW, LW, and total = SW + LW) flux at the top of the atmosphere (TOA) and surface (SFC) between the cloudy sky and the clear sky:
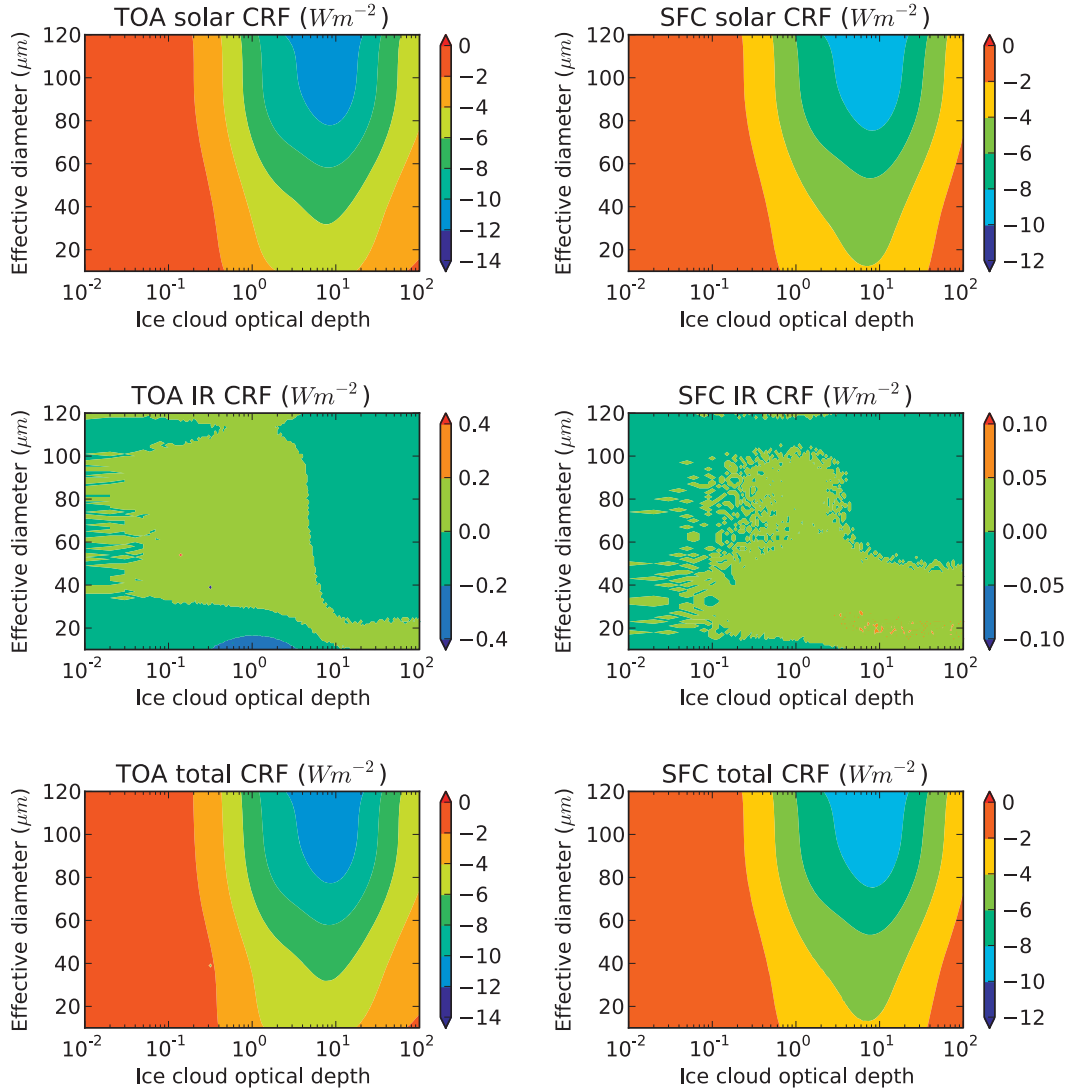
FIG. 3. Ice particle surface roughness effect on (top) SW, (middle) LW, and (bottom) total CRF at SZA = 60° as a function of effective diameter and cloud optical thickness for the Fu–Liou RTM at (left) the TOA and (right) the SFC.

$$\text{CRF} = F_{\text{all sky}} - F_{\text{clear}} = N(F_{\text{cloudy}} - F_{\text{clear}}) \quad \text{and} \quad (7)$$

$$F_{\text{all sky}} = N \times F_{\text{cloudy}} + (1 - N) \times F_{\text{clear}}, \quad (8)$$

where F_{cloudy} and F_{clear} are the net fluxes (downward minus upward) for cloudy (overcast) sky and clear sky, respectively, and N is cloud fraction, assumed to be 1 here. For this test case, an ice cloud layer is located between 12 and 13 km, the solar zenith angle is set to 60°, and the surface is assumed to be black for both the SW and LW (i.e., surface albedo and emissivity are 0 and 1, respectively, at all wavelengths). The CRE is calculated for SR and CS cases with both the Fu–Liou and RRTMG RTMs as the ice cloud optical thickness ranges

from 0.01 to 100 and the D_{eff} ranges from 10 to 120 μm. Figure 2 shows an example of simulated CRE at the TOA and SFC from the Fu–Liou RTM as a function of D_{eff} and the ice cloud optical thickness using the SR ice particle model. Similar results were obtained for RRTMG but are not shown here. The CRE is highly sensitive to the changes in ice cloud optical thickness, while the dependence on D_{eff} is weak. These results are in agreement with the study by Hong et al. (2009).

The simulated ice particle surface roughness effect on CRE (i.e., the difference between the SR and CS CRE) for the Fu–Liou and RRTMG RTMs is shown in Figs. 3 and 4, respectively. The Fu–Liou and RRTMG
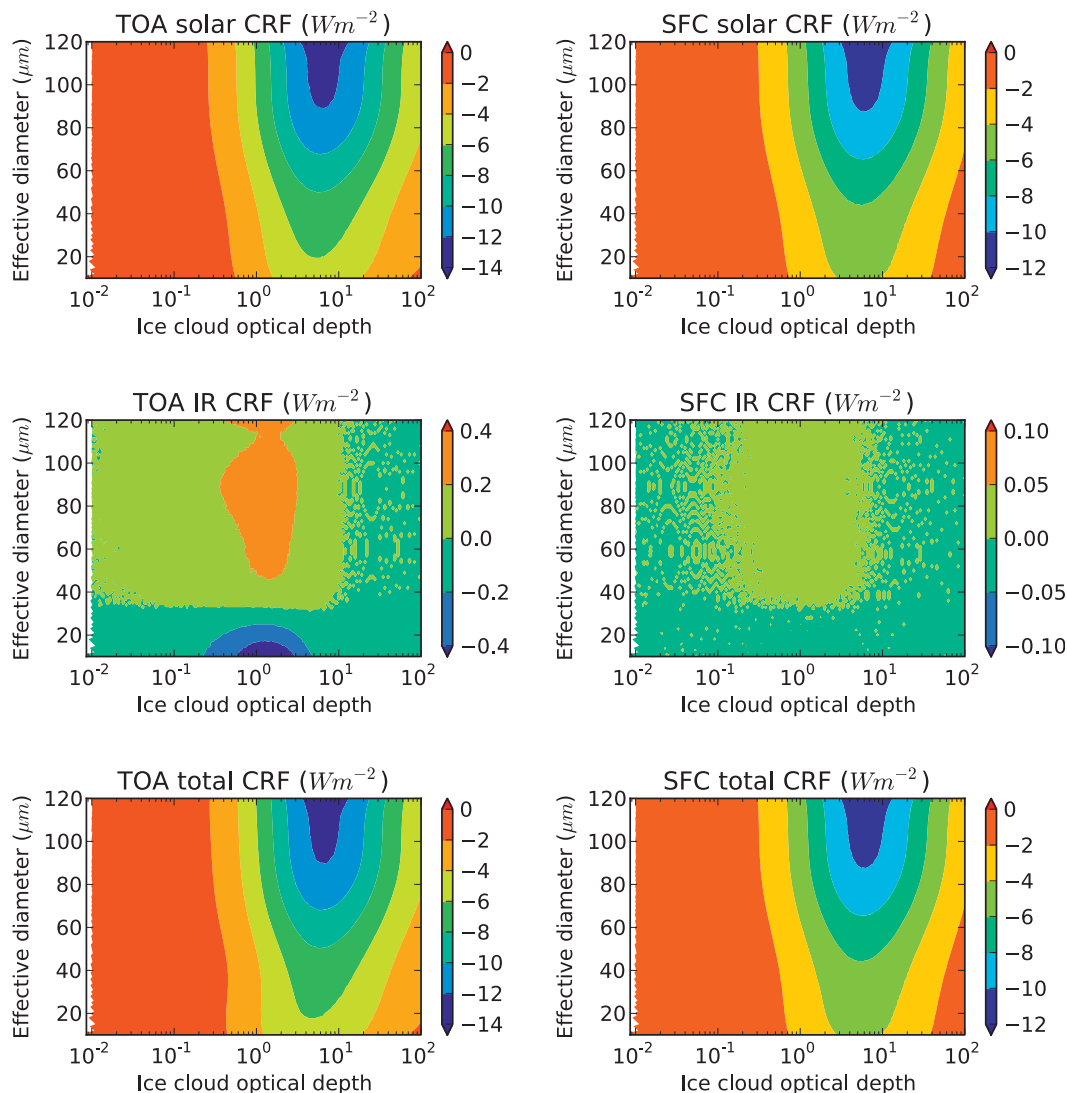
FIG. 4. As in Fig. 3, but for the RRTMG RTM.

results share many common features. First, both RTMs show substantial and dominant roughness effects in the SW while minimal influence in the LW. Second, the most pronounced roughness effects occur when the optical thickness ranges between 3 and 12 for all values of D_{eff}. Beyond this higher value of the optical thickness, the roughness effect decreases for a given particle size. Third, the patterns of the roughness-induced CRE variation with D_{eff} and optical thickness from the two RTMs are quite similar. However, the Fu–Liou RTM tends to have lower roughness-induced SW CRE by around $2\,\mathrm{W\,m^{-2}}$. Moreover, for RRTMG the highest value of the roughness-induced CRE center is skewed toward a smaller ice optical thickness than for the Fu–Liou RTM. These differences could be due to the different band structures of the two RTMs.

b. AGCM modeling results

We now examine the influence of particle roughness on the CRE in the CAM5.1 AGCM. Use of an AGCM in this analysis demonstrates the impact of surface roughness for a broad range of atmospheric profiles that occur through the interaction of the RTM in the AGCM with other model components. More importantly, the AGCM model has the potential to illustrate the dynamical/thermodynamical feedbacks that result from changing only the ice cloud bulk scattering properties. We replace the default ice cloud scattering properties in the version of RRTMG used in CAM5.1 with our new CS and SR parameterizations. CAM5.1 is run for 10 years at $1.9° \times 2.5°$ horizontal resolution and with 31 vertical levels. The model is forced with cyclic
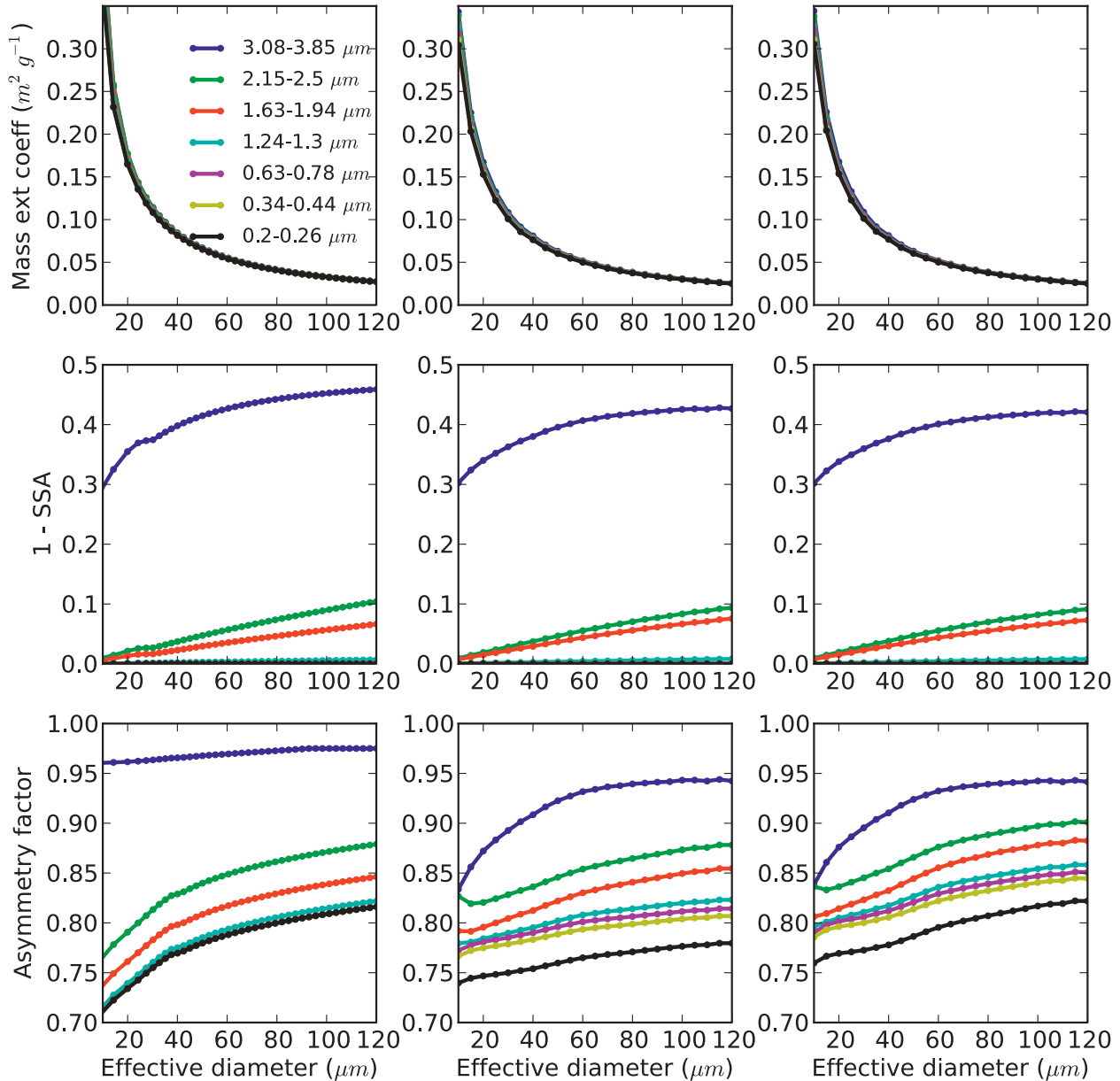
FIG. 5. (top) Mass extinction coefficient, (middle) single-scattering albedo, and (bottom) asymmetry factor as a function of ice particle effective diameter for selected bands in the RRTMG code for (left) the default CAM5 ice cloud model, (middle) the SR ice particle model, and (right) the CS model.

observed sea surface temperature climatology and greenhouse gases to minimize the influence of changing surface and atmospheric conditions and mitigate the influence of any particular weather events in a given year. The results of cloud radiative effect climatology are derived from the 10-yr run.

The optical properties of the new SR and CS ice particle models are compared with those of the default CAM5 (Mitchell et al. 1996, 2006) in Fig. 5. We find considerable differences between the three cases. The

differences between the CAM5 default scheme and our parameterizations are probably not only due to ice particle surface roughness, but other factors as well (e.g., ice particle habits and size distributions assumed in generating the bulk scattering properties). The asymmetry factor shows the largest differences; both the new CS or SR models display substantial differences from the default model currently adopted in CAM5.1. The single-scattering albedo of the near-IR bands tends to decrease for larger effective diameters.
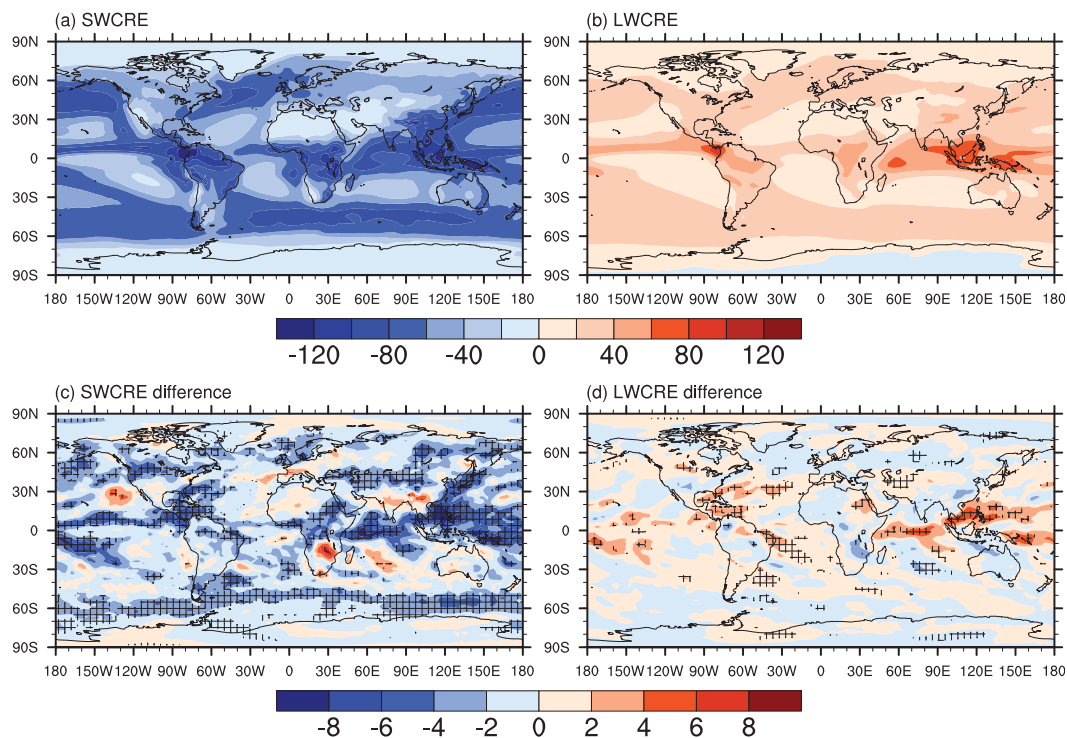
FIG. 6. CAM5.1-simulated 10-yr mean annual total cloud radiative effect (W m^{-2}) and the roughening effects (CRE for the severely roughened case minus that of the smooth case) at the TOA: (a) SW cloud radiative effect (SWCRE), (b) LW cloud radiative effect (LWCRE), (c) roughening effect on SWCRE, and (d) roughening effect on LWCRE. Hatched areas are significant at the 95% significance level.

Figure 6 shows the CAM5.1-simulated 10-yr mean annual total cloud radiative effect as well as the surface roughness effect (again, the difference between the SR and CS cases) on total cloud radiative effect at the TOA. Hatched areas in Fig. 6 are significant at the 95% confidence level. Total cloud radiative effect is shown because the CAM5.1 radiation scheme does not treat different cloud types individually, thus making it impossible to single out the effect of ice clouds. Table 2 summarizes the annual global-averaged SW, LW, and net cloud radiative effect and the roughness effect. A difference of -1.46 W m^{-2} is derived in the net cloud radiative effect owing to the roughening of ice particles. This is a sizeable value that approaches the magnitude of forcing caused by various scenarios of increased CO_2 concentrations.

Results from the 10-yr run also indicate that the spatial and seasonal variations of surface-roughness-induced SW cloud radiative effect are substantial. Zonal averages (Fig. 7) show that strong SW surface roughness effects are found in the tropics and in both hemisphere storm-track regions (Fig. 6). The LW differences are limited mostly to the tropics. March has the largest SW (-2.35 W m^{-2}) and LW (0.67 W m^{-2}) particle roughness effects (Fig. 8). The simulated TOA LW CRE shows

weaker seasonal variations, with a global-averaged value of around 25 W m^{-2} for all seasons.

The single-column RTM simulations shown earlier suggest that roughness has a minimal effect on LW CRE. The CAM5.1 simulations, however, suggest some prominent LW effects in the tropics. This may be indicative of either feedback processes or internal variability in the AGCM that warrant further exploration. Perhaps the perturbation to the SW radiation by ice particle roughening induces changes in regional thermodynamic structure that subsequently lead to persistent local circulation anomalies. In turn, these circulation changes could lead to further changes in the ice cloud properties and, thus, notable LW CRE changes. This suggestion is supported by the fact that surface roughness leads to both positive and negative anomalies in SW CRE in the model (Fig. 6) despite a prominence of SW CRE

TABLE 2. Global annual mean of the SR and CS total cloud radiative effect as well as the roughness effect (SR minus CS) (W m^{-2}).

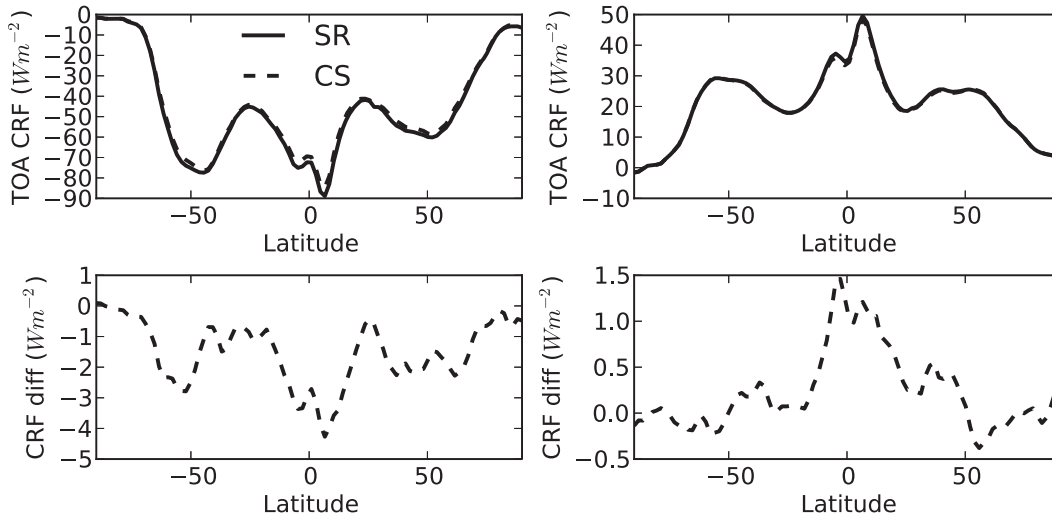|	SR	CS	SR − CS
SW CRE	−55.67	−53.84	−1.83
LW CRE	25.34	24.97	0.37
Net CRE	−30.33	−28.87	−1.46

FIG. 7. (top) The zonal averages of TOA total CRF and (bottom) the ice particle surface roughness effects ($\mathrm{W\,m^{-2}}$) for (left) SW and (right) LW, as simulated by CAM 5.1.

reduction in the single-column calculations (Fig. 3). On a global scale, the roughness effects are smaller but not negligible, which suggests that these feedbacks retain some influence on global LW CRE.

The CAM5.1 AGCM simulation results seem to agree in general with the offline RTM simulation results but are more variable in both sign and magnitude and change with time and geographical locations, indicating potential feedback effects. The CAM5.1 results also provide a way of estimating the effects of ice particle surface roughening on CRE on a global scale, where the global annual average effects on SW and LW CRE are -1.83 and $0.37\,\mathrm{W\,m^{-2}}$ (Table 2), respectively.

4. Conclusions

While there is an increasing awareness of the existence of ice particle surface roughness, few if any studies are available that provide an in-depth analysis of its influence on cloud radiative effect. This paper attempts to provide such a systematic analysis, with new band model parameterizations developed using a new database of ice particle single-scattering properties from the ultraviolet to the far infrared. The new parameterizations employ a set of comprehensive microphysical observations from field campaigns conducted around the world, and adopt ice cloud particle habits similar to those
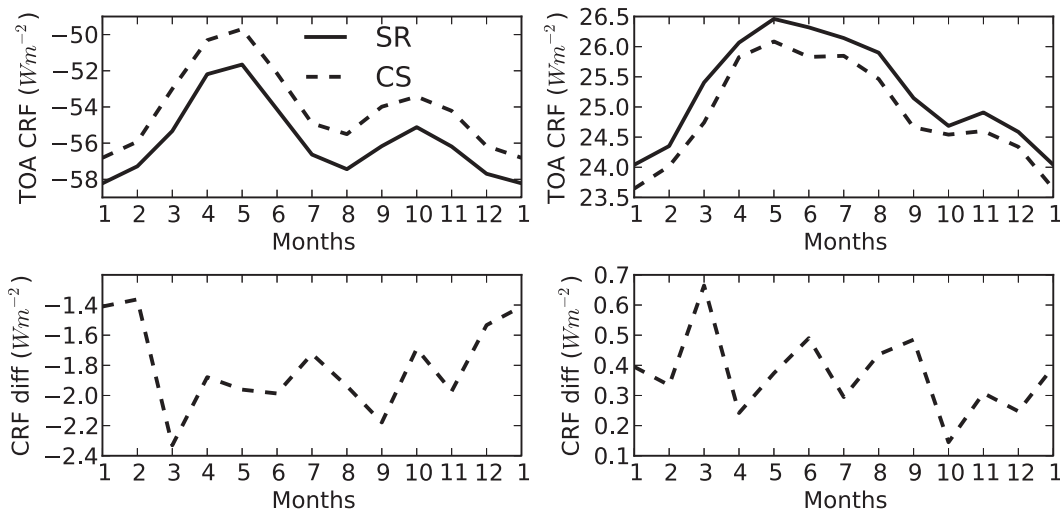

FIG. 8. (top) The annual cycle of TOA total CRF and (bottom) the ice particle surface roughness effects ($\mathrm{W\,m^{-2}}$) for (left) SW and (right) LW, as simulated by CAM 5.1.

implemented in satellite remote sensing studies. The new band parameterizations are derived assuming that all ice particles are either severely roughened (SR) or completely smooth (CS). The CS and SR parameterizations are integrated into the Fu–Liou and RRTMG codes and the National Center for Atmospheric Research (NCAR) Community Atmosphere Model (CAM, version 5.1), which uses a version of the latter algorithm.

The mass extinction coefficient and single-scattering albedo are found to be quite similar between the CS and SR ice crystal models. The primary effect of ice particle surface roughness is in the reduction of the asymmetry factor for rough particles compared with smooth particles of the same size—a reduction that increases with increasing effective diameter D_{eff}. Thus, consideration of the particle surface roughness effect tends to result in decreasing the inferred particle size. Both the uncertainties associated with ice particle size distributions and surface roughness conditions should be considered.

The simulated cloud radiative effect (CRE) is highly sensitive to the variation of ice cloud optical thickness, whereas it is only weakly dependent on D_{eff}. The same is true for the effect of roughness on CRE. The effect of surface roughness in the shortwave (SW) spectrum dwarfs that for the longwave (LW) spectrum. Particle roughness has the most influence (more than $10 \, W \, m^{-2}$ at SZA = 60°) for cases with $D_{eff} \geq 80 \, \mu m$ and where optical thickness ranges between 3 and 12. There are differences between the Fu–Liou and RRTMG RTM results at various D_{eff} and optical thicknesses that might be due to the different spectral bands used in each RTM code.

The AGCM simulations offer a more complete picture of the surface roughness effect on CRE than the RTM results because they provide spatial/seasonal variations and model feedbacks. For example, while the SW cloud radiative effect induced by particle roughness is still large and dominant, the LW forcing in the tropics is larger than expected from the column RTM simulations. The apparent LW radiative effect by particle roughening in the AGCM simulation may be the outcome of thermodynamic feedbacks that modify cloud properties. This is supported by the fact that both positive and negative roughening effects on SW CRE occur in the model; we will investigate this more fully in future work. The global-averaged response due to the adoption of severe particle roughening is estimated to be on the order of $1–2 \, W \, m^{-2}$ for the SW spectrum but much smaller in the LW. Since the global seasonal cloud radiative effect variation is no more than $7 \, W \, m^{-2}$, the contribution from the treatment of ice particle surface roughness is important. A difference of $-1.46 \, W \, m^{-2}$ in the net cloud radiative effect due to the roughening of ice particles is small but is similar in magnitude to the forcing of greenhouse gases under various plausible scenarios. Additional observational and numerical studies (e.g., with other GCMs) are required to shed more light about the importance of crystal roughness on the global radiation budget.

APPENDIX

Representation of Ice Particle Surface Roughness

The ice particle surface roughness is considered in the improved geometric optics method (IGOM; Yang and Liou 1998) used for the calculation of the ice optical property database (Yang et al. 2013). The surface slope of ice particles is represented by a normal distribution following Cox and Munk (1954) who studied the optical effect of sea surface roughness:

$$P(Z_x, Z_y) = \frac{1}{\sigma^2 \pi} \exp\left(-\frac{Z_x^2 + Z_y^2}{\sigma^2} \right), \qquad (A1)$$

where Z_x and Z_y are the slope variations at the particle surface in the x and y directions. By randomly distorting the particle surface slope, the degree of roughness is controlled by the σ parameter. In this study, we select three values of σ with the value of 0.5 denoting the severely roughened particle case, 0.03 denoting the moderately roughened particle case, and 0 for the completely smooth case. Ice particle surface roughness effect is not included for particle size parameters smaller than about 20 where the single-scattering properties are calculated by the discrete dipole approximation method. More discussion about particle surface roughness can be found in Yang and Liou (1998) and Yang et al. (2008).

REFERENCES

Baran, A. J., 2009: A review of the light scattering properties of cirrus. *J. Quant. Spectrosc. Radiat. Transfer,* **110,** 1239–1260.

——, 2012: From the single-scattering properties of ice crystals to climate prediction: A way forward. *Atmos. Res.,* **112,** 45–69.

Baum, B. A., P. Yang, A. J. Heymsfield, S. Platnick, M. D. King, Y. X. Hu, and S. T. Bedka, 2005: Bulk scattering properties

for the remote sensing of ice clouds. Part II: Narrowband models. *J. Appl. Meteor.,* **44,** 1896–1911.

——, ——, ——, C. G. Schmitt, Y. Xie, A. Bansemer, Y.-X. Hu, and Z. Zhang, 2011: Improvements in shortwave bulk scattering and absorption models for the remote sensing of ice clouds. *J. Appl. Meteor. Climatol.,* **50,** 1037–1056.

Bi, L., P. Yang, G. W. Kattawar, B. A. Baum, Y. X. Hu, D. M. Winker, R. S. Brock, and J. Q. Lu, 2009: Simulation of the color ratio associated with the backscattering of radiation by ice particles at the wavelengths of 0.532 and 1.064 um. *J. Geophys. Res.,* **114,** D00H08, doi:10.1029/2009JD011759.

Chance, K., and R. L. Kurucz, 2010: An improved high-resolution solar reference spectrum for earth's atmosphere measurements in the ultraviolet, visible, and near infrared. *J. Quant. Spectrosc. Radiat. Transfer,* **111,** 1289–1295.

C.-Labonnote, L., G. Brogniez, J.-C. Buriez, M. Doutriaux-Boucher, J.-F. Gayet, and A. Macke, 2001: Polarized light scattering by inhomogeneous hexagonal monocrystals: Validation with ADEOS-POLDER measurements. *J. Geophys. Res.,* **106** (D11), 12 139–12 153.

Cole, B., P. Yang, B. A. Baum, J. Riedi, L. C.-Labonnote, F. Thieuleux, and S. Platnick, 2013: Comparison of *PARASOL* observations with polarized reflectances simulated using different ice habit mixtures. *J. Appl. Meteor. Climatol.,* **52,** 186–196.

Comstock, J. M., T. P. Ackerman, and G. G. Mace, 2002: Ground-based lidar and radar remote sensing of tropical cirrus clouds at Nauru Island: Cloud statistics and radiative impacts. *J. Geophys. Res.,* **107,** 4714, doi:10.1029/2002JD002203.

Cox, C., and W. Munk, 1954: Measurement of the roughness of the sea surface from photographs of the sun's glitter. *J. Opt. Amer. Soc,* **44,** 838–850.

Cross, J. D., 1969: Scanning electron microscopy of evaporating ice. *Science,* **164,** 174–175.

Davy, G., and D. Branton, 1970: Subliming ice surfaces: Freezing-etch electron microscopy. *Science,* **168,** 1216–1218.

Ebert, E. E., and J. A. Curry, 1992: A parameterization of ice cloud optical properties for climate models. *J. Geophys. Res.,* **97** (D4), 3831–3836.

Edwards, J. M., S. Havemann, J.-C. Thelen, and A. J. Baran, 2007: A new parameterization for the radiative properties of ice crystals: Comparison with existing schemes and impact in a GCM. *Atmos. Res.,* **83,** 19–35.

Foot, J. S., 1988: Some observations of the optical properties of clouds. Part II: Cirrus. *Quart. J. Roy. Meteor. Soc.,* **114,** 145–164.

Fu, Q., 1996: An accurate parameterization of the solar radiative properties of cirrus clouds for climate models. *J. Climate,* **9,** 2058–2082.

——, 2007: A new parameterization of an asymmetry factor of cirrus clouds for climate models. *J. Atmos. Sci.,* **64,** 4140–4150.

——, and K. N. Liou, 1993: Parameterization of the radiative properties of cirrus clouds. *J. Atmos. Sci.,* **50,** 2008–2025.

——, P. Yang, and W. B. Sun, 1998: An accurate parameterization of the infrared radiative properties of cirrus clouds for climate models. *J. Climate,* **11,** 2223–2237.

Hartmann, D. L., M. E. Ockertbell, and M. L. Michelsen, 1992: The effect of cloud type on Earth's energy balance: Global analysis. *J. Climate,* **5,** 1281–1304.

Heymsfield, A. J., C. Schmitt, A. Bansemer, and C. H. Twohy, 2010: Improved representation of ice particle masses based on observations in natural clouds. *J. Atmos. Sci.,* **67,** 3303–3318.

——, ——, and ——, 2013: Ice cloud particle size distributions and pressure dependent terminal velocities from in situ observations at temperatures from 0° to −86°C. *J. Atmos. Sci.,* in press.

Hong, G., P. Yang, B. A. Baum, A. J. Heymsfield, and K. M. Xu, 2009: Parameterization of shortwave and longwave radiative properties of ice clouds for use in climate models. *J. Climate,* **22,** 6287–6312.

Iacono, M. J., J. S. Delamere, E. J. Mlawer, M. W. Shephard, S. A. Clough, and W. D. Collins, 2008: Radiative forcing by long-lived greenhouse gases: Calculations with the AER radiative transfer models. *J. Geophys. Res.,* **113,** D13103, doi:10.1029/2008JD009944.

Lee, J., P. Yang, A. E. Dessler, B. C. Gao, and S. Platnick, 2009: Distribution and radiative forcing of tropical thin cirrus clouds. *J. Atmos. Sci.,* **66,** 3721–3731.

Liou, K.-N., 1986: Influence of cirrus clouds on weather and climate processes: A global perspective. *Mon. Wea. Rev.,* **114,** 1167–1199.

Lynch, D. K., K. Sassen, D. O. Starr, and G. Stephens, 2002: *Cirrus.* Oxford University Press, 504 pp.

Macke, A., 1993: Scattering of light by polyhedral ice crystals. *Appl. Opt.,* **32,** 2780–2788.

Mitchell, D. L., 2002: Effective diameter in radiation transfer: General definition, applications, and limitations. *J. Atmos. Sci.,* **59,** 2330–2346.

——, A. Macke, and Y. G. Liu, 1996: Modeling cirrus clouds. Part II: Treatment of radiative properties. *J. Atmos. Sci.,* **53,** 2967–2988.

——, A. J. Baran, W. P. Arnott, and C. Schmitt, 2006: Testing and comparing the modified anomalous diffraction approximation. *J. Atmos. Sci.,* **63,** 2948–2962.

Ono, A., 1969: The shape and riming properties of ice crystals in natural clouds. *J. Atmos. Sci.,* **26,** 138–147.

Platt, C. M. R., and Harshvardhan, 1988: Temperature-dependence of cirrus extinction: Implications for climate feedback. *J. Geophys. Res.,* **93** (D9), 11 051–11 058.

——, S. A. Young, P. J. Manson, G. R. Patterson, S. C. Marsden, R. T. Austin, and J. H. Churnside, 1998: The optical properties of equatorial cirrus from observations in the ARM Pilot Radiation Observation Experiment. *J. Atmos. Sci.,* **55,** 1977–1996.

Slingo, A., 1989: A GCM Parameterization for the shortwave radiative properties of water clouds. *J. Atmos. Sci.,* **46,** 1419–1427.

——, and J. M. Slingo, 1988: The response of a general circulation model to cloud longwave radiative forcing. I: Introduction and initial experiments. *Quart. J. Roy. Meteor. Soc.,* **114,** 1027–1062.

Slingo, J. M., and A. Slingo, 1991: The response of a general circulation model to cloud longwave radiative forcing. II: Further studies. *Quart. J. Roy. Meteor. Soc.,* **117,** 333–364.

Takano, Y., and K. N. Liou, 1989: Solar radiative transfer in cirrus clouds. Part I: Single-scattering and optical properties of hexagonal ice crystals. *J. Atmos. Sci.,* **46,** 3–19.

Ulanowski, Z., E. Hesse, P. H. Kaye, and A. J. Baran, 2006: Light scattering by complex ice-analogue crystals. *J. Quant. Spectrosc. Radiat. Transfer,* **100,** 382–392.

——, E. Hirst, P. H. Kaye, and R. Greenaway, 2012: Retrieving the size of particles with rough and complex surfaces from two-dimensional scattering patterns. *J. Quant. Spectrosc. Radiat. Transfer,* **113,** 2457–2464.

Warren, S. G., and R. E. Brandt, 2008: Optical constants of ice from the ultraviolet to the microwave: A revised compilation. *J. Geophys. Res.,* **113,** D14220, doi:10.1029/2007JD009744.

Yang, H. Y., S. Dobbie, R. Herbert, P. Connolly, M. Gallagher, S. Ghosh, S. M. R. K. Al-Jumur, and J. Clayton, 2012: The effect of observed vertical structure, habits, and size distributions on the solar radiative properties and cloud evolution of cirrus clouds. *Quart. J. Roy. Meteor. Soc.,* **138,** 1221–1232.

Yang, P., and K. N. Liou, 1998: Single-scattering properties of complex ice crystals in terrestrial atmosphere. *Contrib. Atmos. Phys.,* **71,** 223–248.

——, ——, K. Wyser, and D. Mitchell, 2000: Parameterization of the scattering and absorption properties of individual ice crystals. *J. Geophys. Res.,* **105** (D4), 4699–4718.

——, B. A. Baum, A. J. Heymsfield, Y. X. Hu, H. L. Huang, S. C. Tsay, and S. Ackerman, 2003: Single-scattering properties of droxtals. *J. Quant. Spectrosc. Radiat. Transfer,* **79,** 1159–1169.

——, L. Zhang, G. Hong, S. L. Nasiri, B. A. Baum, H.-L. Huang, M. D. King, and S. Platnick, 2007: Differences between collection 4 and 5 MODIS ice cloud optical/microphysical products and their impact on radiative forcing simulations. *IEEE Trans. Geosci. Remote Sens.,* **45,** 2886–2899.

——, G. W. Kattawar, G. Hong, P. Minnis, and Y. X. Hu, 2008: Uncertainties associated with the surface texture of ice particles in satellite-based retrieval of cirrus clouds—Part I: Single-scattering properties of ice crystals with surface roughness. *IEEE Trans. Geosci. Remote Sens.,* **46,** 1940–1947.

——, L. Bi, B. A. Baum, K.-N. Liou, G. Kattawar, M. Mishchenko, and B. Cole, 2013: Spectrally consistent scattering, absorption, and polarization properties of atmospheric ice crystals at wavelengths from 0.2 to 100 μm. *J. Atmos. Sci.,* **70,** 330–347.

Zhang, Z., P. Yang, G. W. Kattawar, S.-C. Tsay, B. A. Baum, Y. Hu, A. J. Heymsfield, and J. Reichardt, 2004: Geometrical-optics solution to light scattering by droxtal ice crystals. *Appl. Opt.,* **43,** 2490–2499.

——, ——, ——, J. Riedi, L. C.-Labonnote, B. A. Baum, S. Platnick, and H. L. Huang, 2009: Influence of ice particle model on satellite ice cloud retrieval: Lessons learned from MODIS and POLDER cloud product comparison. *Atmos. Chem. Phys.,* **9,** 7115–7129.